Application of Genetic Optimization Algorithms to Lumped Circuit Modelling of Coupled Planar Coils

Jens Werner[1], Lars Nolle[1], Jennifer Schütt[2]
[1] Jade University of Applied Science Wilhelmshaven/Oldenburg/Elsfleth,
Friedrich-Paffrath-Str. 101, D-26389 Wilhelmshaven,
Email: jens.werner@jade-hs.de, lars.nolle@jade-hs.de
[2] Nexperia Germany GmbH, Stresemannallee 101, D-22529 Hamburg
Email: jennifer.schuett@nexperia.com

KEYWORDS

Coupled planar coils; Common mode filter; Lumped network model; Genetic algorithm; SPICE model

ABSTRACT

In portable electronic devices, like smart phones, coupled planar coils are often used as common mode filters (CMF). The purpose of these CMF is to suppress electromagnetic interference (EMI) between wireless communications systems (e.g. WIFI) and digital high-speed interfaces (e.g. USB 3). A designer of such an electronic device usually carries out a signal integrity (SI) analysis, using models of the system components. There are two alternative ways of modelling the CMF: One is based on matrices (called S-parameters) that describe the behaviour in the frequency domain and are either derived from measurements or simulation tools. The other is using a representation based on lumped circuit networks. In this work, a lumped network is generated manually based on expert knowledge. The advantage of this approach is the reduced number of only passive network components compared to traditional methods that produce much larger networks comprising of many active and passive devices. On the other hand, suitable component values of the lumped network need to be found so that the network exhibits the same frequency response as the physical device. Since there are many interacting parameters to be tuned, this cannot be achieved manually. Hence, a genetic algorithm is applied to this optimisation problem. Two sets of experiments were carried out and a sensitivity analysis has been conducted. It has been shown that the proposed method is capable of finding near optimal solutions within reasonable computation time.

INTRODUCTION

Modern portable electronic devices have to be as compact as possible whilst being efficient. In such devices, miniaturized planar coils can be found, for example, in common mode filters which are built directly into integrated circuits.

For the design of these coils, sophisticated simulation tools based on the method of moments (Keysight, 2016; Harrington, 1968) are often used. Usually, these simulations return frequency dependent scattering parameters (S-parameters, (Pozar, 2012)). This is a black-box approach describing the electrical behaviour in the frequency domain at the ports (or: terminals) of the device without revealing details about the physics of the internal structure (1).

$$[\underline{S}] = \begin{bmatrix} \underline{S}_{dd,11} & \underline{S}_{dd,12} & \underline{S}_{dc,11} & \underline{S}_{dc,12} \\ \underline{S}_{dd,21} & \underline{S}_{dd,22} & \underline{S}_{dc,21} & \underline{S}_{dc,22} \\ \underline{S}_{cd,11} & \underline{S}_{cd,12} & \underline{S}_{cc,11} & \underline{S}_{cc,12} \\ \underline{S}_{cd,21} & \underline{S}_{cd,22} & \underline{S}_{cc,21} & \underline{S}_{cc,22} \end{bmatrix} \quad (1)$$

In matrix (1) all elements are complex valued and frequency dependent. The two parameters $\underline{S}_{dd,21}$ and $\underline{S}_{cc,21}$ describe the transmission characteristics between the two ports for two different modes of operation, differential mode (dd) and common mode (cc). Those parameters with mixed indices ($\underline{S}_{dc,ij}$ and $\underline{S}_{cd,ij}$) are relevant for the conversion from one mode to another; for that reason the elements of matrix (1) are also called mixed-mode S-parameters (Bockelman and Eisenstadt, 1995). For passive and reciprocal devices the forward and reverse transmission parameters $\underline{S}_{x,21}$ and $\underline{S}_{x,12}$ are identical. The focus in this work is on $\underline{S}_{dd,21}$ and $\underline{S}_{cc,21}$, which are the most important parameters for real world applications.

Fig. 1 shows the two modes of operation for a two-port device, like a CMF. The two ports are denoted by the indices 1 and 2 as used in (1). In differential mode (Fig. 1 a)) opposing currents (I_+, I_-) are applied to the pins of port 1. There is no current in the ground path ($I_{gnd} = 0$). The transfer characteristics of this mode from port 1 to port 2 is described by $\underline{S}_{dd,21}$.

In common mode (Fig. 1 b)), the pins of port 1 are driven commonly, resulting in a return current of the same amplitude in the ground path. The transfer characteristics of this mode from port 1 to port 2 is described by $\underline{S}_{cc,21}$.

However, sometimes a designer needs to analyse the behaviour in the time domain as well. Here, an equivalent circuit model is usually required, which exhibits the

Proceedings 31st European Conference on Modelling and
Simulation ©ECMS Zita Zoltay Paprika, Péter Horák, Kata Váradi,
Péter Tamás Zwierczyk, Ágnes Vidovics-Dancs, János Péter Rádics (Editors)
ISBN: 978-0-9932440-4-9/ ISBN: 978-0-9932440-5-6 (CD)

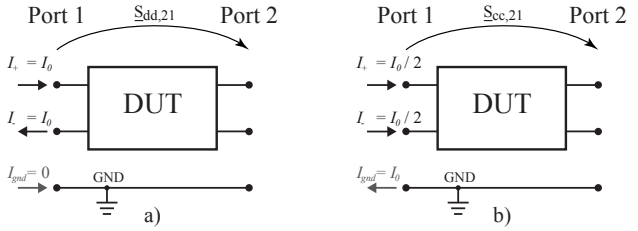

Fig. 1. Differential mode and common mode currents of a two-port device under test (DUT).

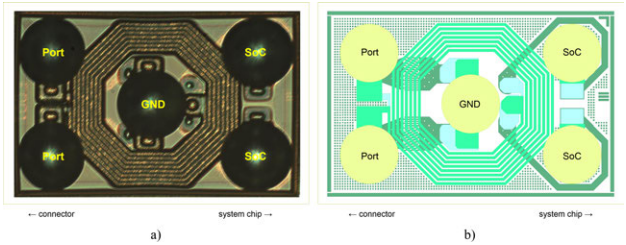

Fig. 2. Planar top view: a) die photograph; b) layout in EM tool (Werner et al., 2016).

same characteristics as the coil in both, the time and the frequency domain. In general, broadband SPICE generators (Simulation Program with Integrated Circuit Emphasis) produce networks of idealised components (so called lumped networks), which exhibit the required behaviour at their terminals (Stevens and Dhaene, 2008). In practice, these networks consist of a large number of active and passive components, which do not resemble the physics of the coils. The approach presented in this paper uses expert knowledge to generate a network which is closer to the actual physics whilst being much smaller. The challenge in this approach is that the component values of this network have to be determined. However, even for networks with few components the search space is too vast to find the optimum values manually. Therefore, a computational optimisation approach is used in this work and applied to a common mode filter (CMF) that consists of two planar coupled coils.

APPLICATION

In high-speed differential data lines (e.g. USB, SATA, PCIe) the spectrum used overlaps with wireless radio communication bands (e.g. GSM, LTE, WIFI). Electromagnetic interference (EMI) for example caused by USB 3 data lines can potentially disturb wireless applications in the 2.4 GHz band as reported in (Intel, 2012; Chen et al., 2013; USB, 2016). In the same manner, the spectrum of an USB 2 signal might interfere with the GSM 900 MHz downlink spectrum (Werner et al., 2015). This can cause a degradation of the receiver sensitivity in a mobile phone.

As wireless and wired signals utilise the same frequency band, a low pass filter can not be used to reduce unwanted interference from data lines into an antenna and finally the receiver. Instead, a common mode filter is applied. The purpose of a CMF is to suppress unwanted common mode (CM) currents on the data lines, since those currents are responsible for the EMI. Ideally, the differential mode (DM) currents of the wanted high-speed signals are not affected. Typically, CMFs are built using two coupled coils.

Common mode filter with on-chip planar coils

Fig. 2 a) shows the top view on a planar copper coil as part of an integrated on-chip CMF (Werner et al., 2016). In addition Fig. 2 b) presents the layout view from the EM design tool (Keysight, 2016).

For all kind of digital high-speed transmission systems, a signal integrity (SI) analysis is performed in the time domain. This involves the simulation of a large number of transmitted data bits and the evaluation of their electrical characteristics at each sampling point in the time domain. The segmented and overlapped representation of this time domain data is known as eye diagram (Gao et al., 2010; Ahmadyan et al., 2015). Here, the simulation in the time domain benefits from an exact and compact SPICE model of the involved planar structures.

Circuitry

The fundamental common mode filtering is achieved by two planar copper coils. The chosen device-under-test (DUT) provides furthermore ESD protection in order to avoid destruction of the sensitive CMOS system-on-chip (SoC). This protection is accomplished by two low-voltage triggered semiconductor controlled rectifiers (LVTSCR) which will shunt the current of an ESD pulse into the ground (GND) connection. These LVTSCR are depicted by the diode symbols in Fig. 3. In an real application, like a smart phone with USB 3 connector, the diodes would be mounted towards the external interface, in order to protect the SuperSpeed receive (SSRX) or transmit (SSTX) signal lines.

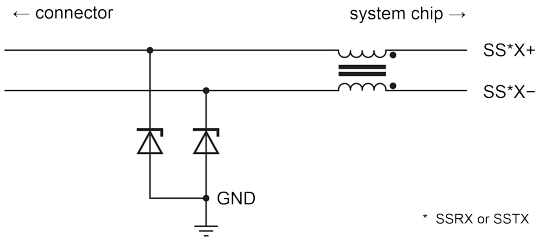

Fig. 3. Functional diagram (Werner et al., 2016).

Physical realisation

The filter device is fabricated in a planar bipolar semiconductor process with two metal layers made by aluminium. In addition, three layers of polyimide and three layers of copper are added on top of the planar wafer. Two of these copper layers form the planar coupled coils. There is no plastic package surrounding the silicon die, instead the device is attached with solder balls and manufactured as wafer level chip scale package. The contact side of the CMF is depicted in Fig. 2 a). The five solder balls marked with "Port", "SOC" and "GND" can be clearly identified as well as

the octagonal shaped coil around the GND ball. The layout of this CMF, generated in an EM simulation tool, is shown in Fig. 2 b). It marks in the same manner the five ball pads. Due to the top view perspective only the upper coil layer can be seen.

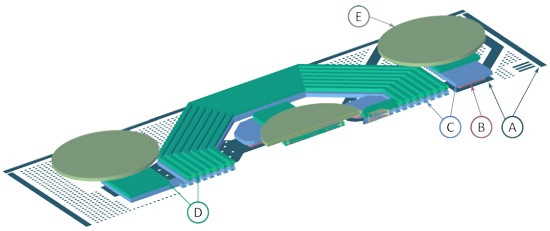

Fig. 4. Cross sectional view from EM simulation tool showing all metal layers (without solder balls) (Werner et al., 2016).

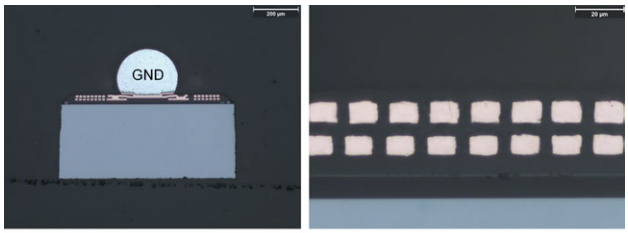

Fig. 5. Cross sectional view from scanning electron microscope: a) symmetric cut through GND ball; b) detailed view on upper and lower copper coil layer (Werner et al., 2016).

The cross sectional view in Fig. 4 provides a more detailed perspective into the structure:

The symbol "A" marks the top level metal of the semiconductor process which is needed to implement the basic semiconductor schematic. Furthermore it provides the interconnection to the 3-metal/3-polyimide-process. "B" denotes the interconnect between first copper layer and top aluminium layer. "C" and "D" mark the two copper layers which are the core of this common mode filter. These layers determine dominantly the inductance and resistance of the coils. The third copper layer, marked by "E", enables the so-called under bump metal, a drop area for the solder ball.

Fig. 5 depicts the physical cross section of the manufactured CMF. Fig. 5 a) shows a cross section that is orthogonal to the cut plane as shown in Fig. 4. This picture gives a good impression about the real relation between silicon thickness, solder ball and copper structures. As it can be seen in Fig. 5 b) the planar coil windings are rectangular shaped with a larger width than height and a spacing in the same range as the height. The typical spacing between the coil windings is 5 µm.

STRUCTURAL MODELLING

As mentioned above, when a designer needs to analyse the behaviour of an entire system in the time domain, for example for a signal integrity analysis, a lumped network can offer a solution. In contrast to transforming S-parameters directly into the time domain, this approach has the advantage that causality, passivity and reciprocity (Triverio et al., 2007) are inherently fulfilled.

One of the simplest schematic diagrams, one could think of, that represents the electric function as shown in Fig. 3 is given in Fig. 6: The two planar coils are represented by inductors L1a and L1b, while the magnetic coupling is modelled by the coupling coefficient kval. Electric and dielectric losses are summed up into the two resistors R1a, R1b. The two LVTSCRs are in a high impedance state as long as no ESD pulse is discharged. Thus their junction capacitance (Cval) is the dominant characteristic to be considered here. Finally, this simple lumped circuit model is described by only four parameters: Lval, Rval, kval and Cval. After a swift manual tuning of those four values, a comparison of the tuned model and the measured frequency response of the CMF was done.

Both, differential and common mode response are calculated and plotted by their magnitude and phase in Fig. 7. While the phase is matched for frequencies up to around 1 GHz, the amplitude response starts to show significant deviation already at ≈ 600 MHz. Since this CMF is applied to an USB 3 signal with 5 GBit/s, it is obvious that this model is not suited to perform a proper signal integrity (SI) analysis in the time domain. A more complex, yet still comprehensible model is given in Fig. 8.

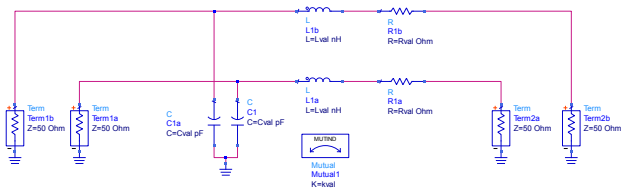

Fig. 6. Basic schematic diagram of common mode filter with ESD protection.

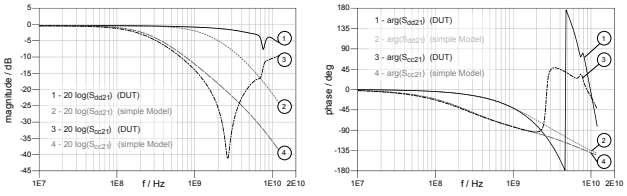

Fig. 7. Amplitude and phase response of CM and DM: Measured data of DUT vs. simulated response of simple lumped model.

The core of this model is a set of seven cascaded pairs of coupled coils. They are meant to mimic the 7.5 windings of the DUT. From the outer to the inner windings it is assumed that resistance will decrease and inductance will increase slightly. This is modelled by a factor c_1, applied from one segment to another. Each single inductor is characterised by its inductance ($\propto L_1$) and its resistance ($\propto R_1$). The magnetic coupling k_2 is assumed to be identical for all paired inductors. The total capacitance between upper and lower copper layer of the coils is described by six capacitors and two parameters: the fundamental capacitance C_1 and another scaling factor c_2. Inter-winding capaci-

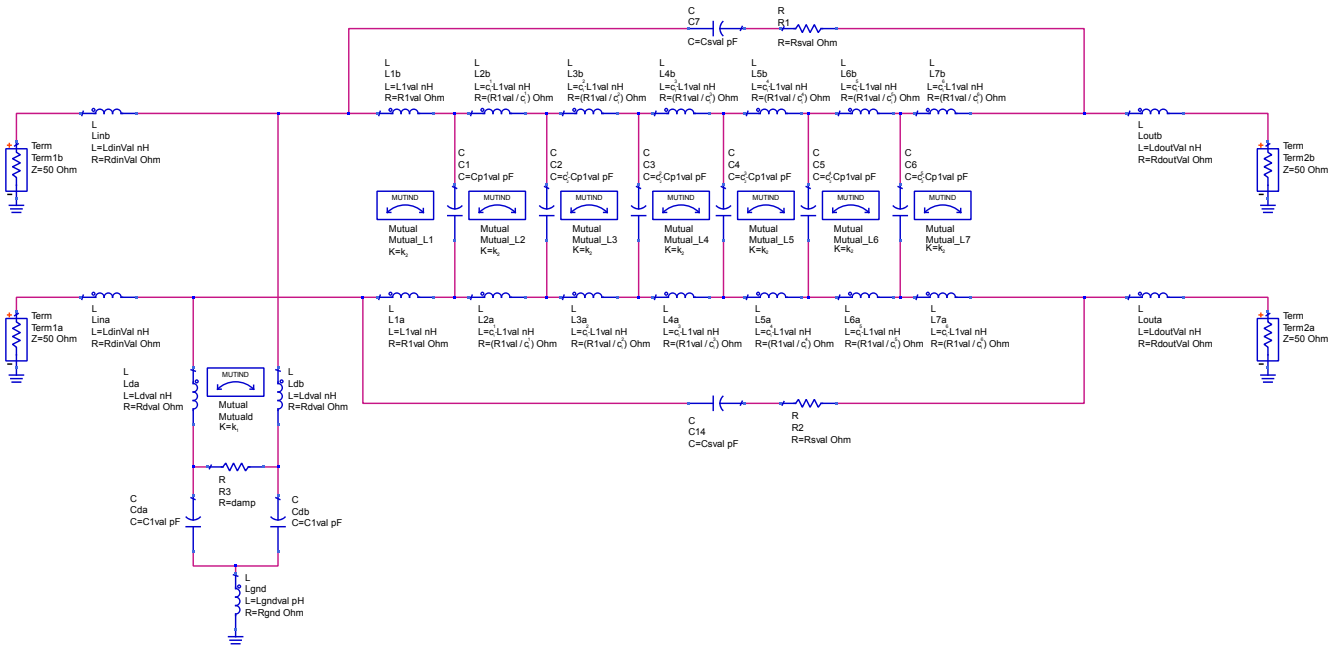

Fig. 8. Lumped element circuit diagram as used in the simulation and optimisation process.

tance is neglected. Cross-talk from the CMF input to the output is modelled by a series network C_s, R_s on each signal line. In general the impedance of each signal trace at the terminals is modelled by a series resistor and inductor. The values of these components (L_{in}, R_{in} and L_{out}, R_{out}) may differ for input and output since the LVTSCRs are only present at one side. For the junction capacitance of the LVTSCRs the capacitance C_d is used. The impedance of the inter-connect metal is modelled by L_d, R_d while the shunt resistor R_{ds} represents losses and is applied to tune the quality factor of the LC-circuit formed by L_c and C_d. Finally, the connection to the GND ball is defined by L_{gnd} and R_{gnd}. The challenge now is to determine the 19 component values so that the behaviour of the lumped model matches that of the measurements from the actual device. This is achieved in this work by computational optimisation.

MODEL OPTIMISATION

In computational optimisation a given error function f is driven towards an extreme value by a direct search algorithm in an iterative process (see Fig. 9). The error function maps an error value onto a given design vector $\boldsymbol{d}$. Here, this vector contains the 19 component values to be optimised (2).

The error e is then used by the optimisation algorithm to create new candidate solutions, i.e. design vectors.

The challenge in this research is to find an optimum design vector $\boldsymbol{d}'$ that produces a DM and CM frequency response as close as possible to the measured data of the DUT by minimising the error function (3).

$$\boldsymbol{d} = \{L_{in}, R_{in}, L_d, R_d, k_1, R_{ds}, \cdots, L_{out}, R_{out}\}^T \quad (2)$$

$$\boldsymbol{d}' = \arg\min f(\boldsymbol{d}) \quad (3)$$

The error function and the algorithm used in this work are described below.

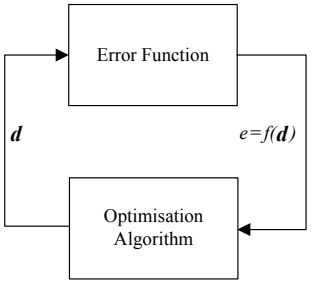

Fig. 9. Optimisation loop

Error function

For the problem at hand the error is defined as difference between a calculated and a measured frequency response (5)-(13). Such a difference can be calculated by comparing both graphs at arbitrary discrete frequencies. Since the given frequency responses exhibit a strong variation at rather high frequencies, the sampling rates have been chosen differently for low and high frequencies according to (4), see Fig. 10.

Since the interest is in both, differential mode and common mode response, two error terms e_{DM} and e_{CM} are combined using the weighted sum (5).

Both frequency responses are complex valued, i.e. amplitude and phase have to be optimised. With (6) and (10) again a weighted sum is used to combine these contributions to the error value.

$$f(i) = \begin{cases} 10\,\mathrm{MHz} \cdot \left(10^{\frac{1}{10}}\right)^{i} & \forall\, 0 \le i \le 27, i \in \mathbb{N} \\ 5\,\mathrm{GHz} \cdot \left(10^{\frac{1}{92}}\right)^{i-27} & \forall\, 28 \le i \le 62, i \in \mathbb{N} \end{cases} \tag{4}$$

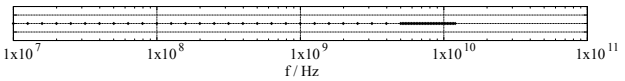

Fig. 10. Spacing of the 63 discrete frequency points for the error function.

$$e = \frac{1}{2} \cdot e_{DM} + \frac{1}{2} \cdot e_{CM} \tag{5}$$

$$e_{DM} = \sum_{i=0}^{62} 10 \cdot e_{DM}^{mag}(i) + e_{DM}^{phase}(i) \tag{6}$$

$$e_{DM}^{phase}(i) = \left|\arg\left(S_{dd,21}^{DUT}(f(i))\right) - \arg\left(S_{dd,21}^{opt}(f(i))\right)\right| \tag{7}$$

$$e_{DM}^{mag}(i) = \begin{cases} 5 \cdot \Delta_{DM}^{mag}(i) \text{ if} & i < 54 \wedge \Delta_{DM}^{mag}(i) \ge 0.1 \\ 1 \cdot \Delta_{DM}^{mag}(i) \text{ else} \end{cases} \tag{8}$$

$$\Delta_{DM}^{mag}(i) = \left|20 \cdot \log\left(\left|\frac{S_{dd,21}^{DUT}(f(i))}{S_{dd,21}^{opt}(f(i))}\right|\right)\right| \tag{9}$$

$$e_{CM} = \sum_{i=0}^{62} 10 \cdot e_{CM}^{mag}(i) + e_{CM}^{phase}(i) \tag{10}$$

$$e_{CM}^{phase}(i) = \left|\arg\left(S_{cc,21}^{DUT}(f(i))\right) - \arg\left(S_{cc,21}^{opt}(f(i))\right)\right| \tag{11}$$

$$e_{CM}^{mag}(i) = \begin{cases} 2 \cdot \Delta_{CM}^{mag}(i) \text{ if} & i < 8 \\ 1 \cdot \Delta_{CM}^{mag}(i) \text{ else} \end{cases} \tag{12}$$

$$\Delta_{CM}^{mag}(i) = \left|20 \cdot \log\left(\left|\frac{S_{cc,21}^{DUT}(f(i))}{S_{cc,21}^{opt}(f(i))}\right|\right)\right| \tag{13}$$

Computational Optimisation

For engineering design optimisation, it is recommended to use a fixed number of decimal places (Nolle et al., 2016). Thus, the optimisation problem was transformed into a discrete optimisation problem. For this, a genetic algorithm (GA) (Goldberg, 1989) was used to minimise the error function (Fig. 9).

Genetic algorithms are discrete optimisation algorithms which simulate the evolutionary mechanism found in nature by using heredity and mutation. They were first introduced in 1975 by Holland (Holland, 1975) who also provided a theoretical framework for genetic algorithms, the Schemata Theorem.

For the optimisation problem under consideration, an integer coded genetic algorithm (Abbas, 2006) was used. Fig. 11 shows the chromosome structure employed.

Fig. 11. Chromosome structure used.

Each gene holds integer numbers from the range 1...2000 and is decoded into its phenotype by multiplication with a scaling factor and addition of an offset value in order to represent the fractional component values of the network. This results in a lower limit and an upper limit for the search space of each component value as listed in Table I.

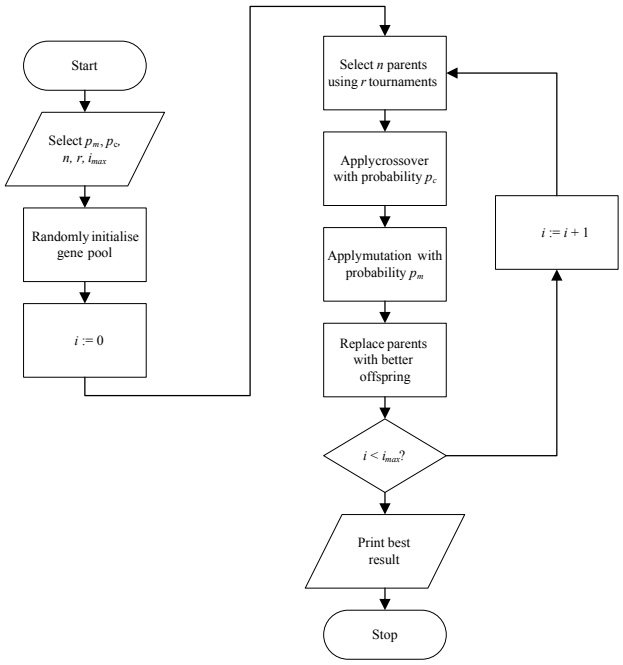

Fig. 12. Flowchart of the genetic algorithm used.

Fig. 12 shows a flowchart of the basic algorithm. After choosing the mutation probability p_m, the crossover probability p_c, the number n of individuals in the gene pool, the number r of tournaments used for the selection of one parent, and the maximum number of iterations i_{max}, the gene pool is randomly initialised. In each of the n generations, parents from the current generation are selected for the mating pool using tournament selection with r tournaments each (Miller and Goldberg, 1996). Then, uniform crossover (Syswerda, 1989) is used with probability p_c to produce offspring from the mating pool. After power mutation (Deep and Thakur, 2007) is applied to the offspring with the probability p_m, parents that perform worse than their offspring are replaced by their offspring. The algorithm terminates after i_{max} generations.

The next section provides the results of the experiments conducted.

TABLE I: Optimisation parameters and results of the second simulation set with $N = 25$ runs

Parameter	1	2	3	4	5	6	7	8	9	10	11	12	13	14	15	16	17	18	19
Name	L_{in}	R_{in}	L_d	R_d	k_1	R_{ds}	C_d	L_{gnd}	R_{gnd}	L_1	R_1	k_2	c_1	C_p	c_2	R_s	C_s	L_{out}	R_{out}
unit	nH	Ohm	nH	Ohm	1	kOhm	pF	pH	Ohm	nH	Ohm	1	1	pF	1	Ohm	pF	nH	Ohm
Lower limit	0.5	0.0	1.0	2.0	-1.0	2.0	0.0	200	3.0	1.0	0.0	0.4	1.0	0.0	0.6	100	0.0	0.5	3.0
Upper limit	2.5	2.0	7.0	14.0	-0.4	4.0	2.0	600	5.0	7.0	2.0	1.0	1.8	2.0	1.0	500	2.0	2.5	9.0

EXPERIMENTS

For the experiments, the number of generations was set to $i_{max} = 20{,}000$ and the population size to $n = 1000$. The crossover probability was chosen to be $p_c = 0.6$ and the mutation probability was $p_m = 0.001$. Five individuals competed in each tournament. All these parameters were determined empirically and have been applied successfully in previous work (Werner and Nolle, 2016). With respect to the search space of the optimisation variables, two sets of experiments were conducted, each with 25 simulation runs.

The error values are normalized by the lower bound of the error values, i.e. 880. Fig. 13 shows a convergence plot for the average errors and the best solutions of each generation over 25 runs. It can be observed that most populations have converged after approximately 4000 generations.

After the first set of 25 runs it could be observed that 14 runs ended with an L_{out} value of 0 nH, which is exactly the lower limit of this optimisation parameter. The solutions related to this result are labelled group I. The other eleven solutions, denoted group II, resulted in 0.7 nH$< L_{out} <$1.3 nH. Results for both groups and the measured data are shown in Fig. 14. Even though the group I solutions yield a lower error value than those of group II they show a rather large deviation in the magnitude against the response of the DUT. Since the response of group II is more desirable and the value of $L_{out} = 0$ nH is physically unreasonable, the lower limit for this parameter was adjusted to 0.5 nH for the second set of 25 runs.

After the adjustment of the lower limit for L_{out} a clustering could still be observed; solutions belonging to one cluster converged towards the (new) lower limit whereas the others converged towards 1.15 nH. Therefore, the solutions were analysed separately for each cluster (Table II). Both clusters of this second set were labelled group I and II in the same way as it was done in the first set: Group I solutions are the ones that converged towards the lower limit of L_{out}, the remaining solutions belong to group II.

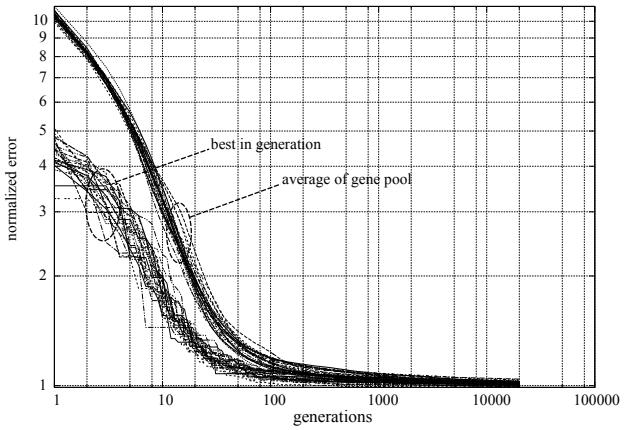

Fig. 13. Convergence plot of 25 optimisation runs. The error value is normalized by 880.

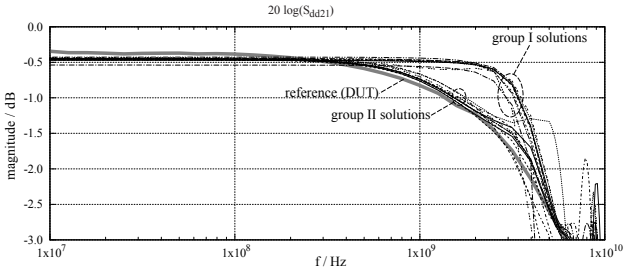

Fig. 14. Differential mode frequency response of DUT and results of first optimisation run. Two groups of local optima can be identified.

DISCUSSION

The best solution of group II (Table II) was used as overall solution and compared with the measurement data. Fig. 15 and Fig. 16 depict the frequency responses for both, the differential and the common mode, of the simulation respectively the measured data.

Fig. 15 shows that, for the differential mode, amplitude $|S_{dd,21}|$ and phase $\arg(S_{dd,21})$ are matched very well up to approximately 7 GHz. At the resonance frequency of 7.6 GHz, amplitude and phase show a certain deviation and above 9 GHz the model and measurements do not agree. For the common mode (Fig. 16) the amplitude response $|S_{cc,21}|$ is matched quite well in general with the exception of the resonance frequency around 2.5 GHz and frequencies above 5 GHz.

The phase $\arg(S_{cc,21})$ is matched accurately up to 600 MHz. At higher frequencies it still follows the measurements in principle, but with a higher error.

For both modes, the chosen model matches the measurements well in amplitude and phase over wide frequency ranges. This can be observed in more detail from Fig. 17, which shows the logarithmic magnitude of the complex differences. For frequencies below 7 GHz both differences are below -20 dB.

In order to analyse the complexity of this optimisation problem, a sensitivity analysis of the component values has been performed. In the optimum solution from group II (best (II) in Table II) each element of the optimum design vector $\boldsymbol{d}'$ is varied one at a time by a step of $(h \cdot d'_i)$ with $h = 1 \cdot 10^{-3}$. This allows to approximate the derivative of the error function with respect

TABLE II: Optimisation parameters and results of the second simulation set with $N = 25$ runs

Parameter	1	2	3	4	5	6	7	8	9	10	11	12	13	14	15	16	17	18	19
Name	L_{in}	R_{in}	L_d	R_d	k_1	R_{ds}	C_d	L_{gnd}	R_{gnd}	L_1	R_1	k_2	c_1	C_p	c_2	R_s	C_s	L_{out}	R_{out}
unit	nH	Ohm	nH	Ohm	1	kOhm	pF	pH	Ohm	nH	Ohm	1	1	pF	1	Ohm	pF	nH	Ohm
Best (I)	0.96	1.01	3.10	2.01	-.86	2.24	0.07	494	3.06	4.27	0.03	0.87	1.06	0.19	0.86	233	0.05	0.50	3.10
Mean (I)	0.81	0.55	4.38	2.97	-.66	3.17	0.06	318	3.03	3.58	0.09	0.84	1.13	0.15	0.89	239	0.06	0.89	3.53
Std. dev. (I)	0.26	0.41	0.45	1.43	0.06	0.34	0.01	98	0.06	0.69	0.08	0.02	0.06	0.02	0.03	13	0.00	0.42	0.42
Best (II)	0.60	0.45	4.10	2.02	-.60	2.60	0.06	210	3.01	2.65	0.01	0.82	1.22	0.13	0.90	226	0.06	1.12	3.78
Mean (II)	0.60	0.48	4.45	2.24	-.63	3.04	0.06	312	3.02	2.76	0.07	0.82	1.20	0.13	0.91	227	0.06	1.15	3.59
Std. dev.(II)	0.08	0.28	0.32	0.48	0.04	0.27	0.00	125	0.02	0.17	0.05	0.00	0.02	0.01	0.02	5	0.00	0.16	0.31

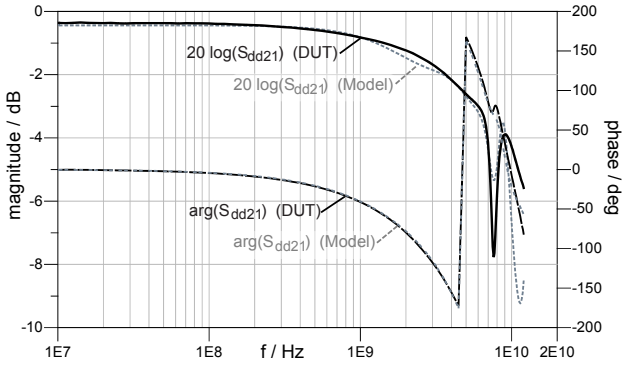

Fig. 15. Differential mode frequency response $S_{dd,21}$ of DUT and model.

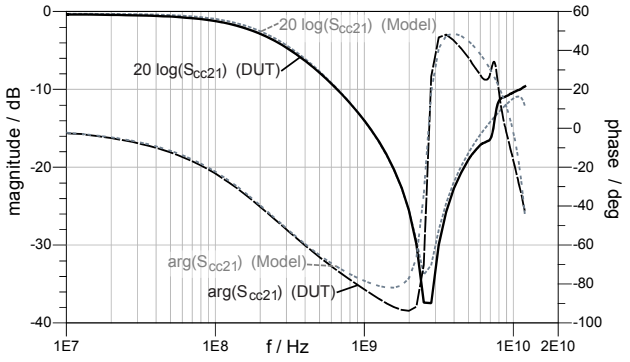

Fig. 16. Common mode frequency response $S_{cc,21}$ of DUT and model.

to the ith component of $\boldsymbol{d}$ (Bischof and Carle, 1998).

$$\left.\frac{\partial f(\boldsymbol{d})}{\partial d_i}\right|_{\boldsymbol{d}=\boldsymbol{d}'} \approx \frac{f(\boldsymbol{d}' + h \cdot d_i' \cdot \boldsymbol{e}_i) - f(\boldsymbol{d}')}{h \cdot d_i'} \qquad (14)$$

Here, f is the error function and $\boldsymbol{e}_i$ is the ith Cartesian basis vector. The analysis is done for both error functions of the differential and the common mode.

Table III presents the sensitivities for the common mode (CM sens.) and the differential mode (DM sens.) for each component. It can be observed that some sensitivities are equal or close to zero, i.e with respect to the corresponding parameter, a (local) optimum has been reached, whereas others show a significant deviation from zero. This indicates that further improvements might be possible.

Another interesting aspect is that in the common mode there is no electric current through components 6, 14 and 15, meaning that their respective component values are irrelevant. Likewise in differential mode,

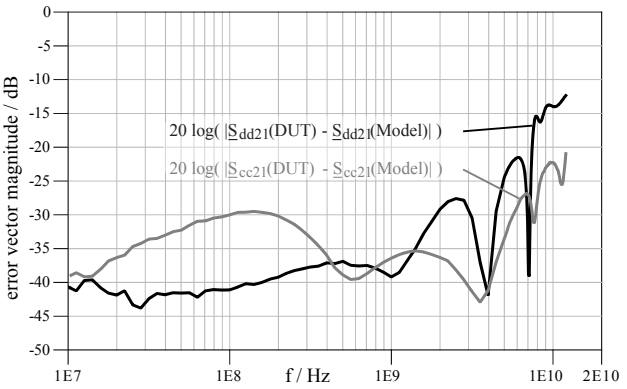

Fig. 17. Error vector magnitude for differential and common mode frequency response comparing DUT and model.

TABLE III: Sensitivity analysis of the component values of the optimum solution from group II.

Nr	Comp.	CM sens.	DM sens.
1	L_{in}	-355.5	290.9
2	Rin	-6.5	2.4
3	Ld	-0.1	350.9
4	Rd	3.4	-0.8
5	k1	-1.3	-987.3
6	Rds	0.0	-0.01
7	Cd	-2418.6	28330.8
8	Lgnd	0.0	0.0
9	Rgnd	6.7	0.0
10	L1	39.2	-264.2
11	R1	-30.1	1.9
12	k2	67.0	-353.7
13	c1	313.1	-324.4
14	Cp	0.0	-5829.7
15	c2	0.0	-281.3
16	Rs	-0.4	0.2
17	Cs	2041.2	-707.8
18	Lout	-89.1	-748.3
19	Rout	-7.6	0.9

no current is traversing through components 8 and 9, hence they have no effect on the resulting frequency responses. Both observations agree with the actual physics of the network.

CONCLUSION AND FUTURE WORK

In this work, the behaviour of a coupled coil device was modelled by a lumped element network. The advantage is that this model describes the device not only in the frequency domain, but also in the time domain. The latter is important for the signal integrity analysis of high-speed interfaces, like USB 3. The topology of the network was generated manually using expert knowledge. It should be noted that the modelling of a complex physical device by a simplified (lumped) net-

work can never achieve an exact representation but only a close approximation. The challenge of this approach is that the component values of the network have to be determined.

The aim is to find a local optimum which produces a frequency response as close as possible to the DUT characteristic.

Since this optimisation problem is complex, a computational optimisation method, namely a genetic algorithm, was employed. The solution found produced good matching between the measurements and model responses for frequencies up to approximately 7 GHz. Whilst this agreement would be sufficient for many applications it is not adequate enough to be applied to interfaces with data rates of 5 Gbit/s and above. This is due to the fact that the fifths harmonic of the fundamental wave of the signal ($5 \cdot 2.5$ GHz) is of importance.

The fact that the results were clustered into two groups indicates that the global optimum was not found. This assumption is support by the results from the sensitivity analysis presented here.

The next stage of this research will foucs on three different aspects: tuning the error function, adjusting the GA control parameters and testing alternative optimisation algorithms.

REFERENCES

Bluetooth & USB 3.0 - A guide to resolving your Bluetooth woes, 2016. URL `http://www.bluetoothandusb3.com/`. [2017-03-30].

H. M. Abbas. Accurate resolution of signals using integer-coded genetic algorithms. In *2006 IEEE International Conference on Evolutionary Computation*, pages 2888–2895, July 2006.

S. N. Ahmadyan, C. Gu, S. Natarajan, E. Chiprout, and S. Vasudevan. Fast eye diagram analysis for high-speed CMOS circuits. In *2015 Design, Automation Test in Europe Conference Exhibition (DATE)*, pages 1377–1382, March 2015.

Christian Bischof and Alan Carle. Automatic differentiation principles, tools, and applications in sensitivity analysis. In *Second International Symposium on Sensitivity Analysis of Model Output*, pages 33–36, April 1998. ISBN 92-828-3498-0.

D. E. Bockelman and W. R. Eisenstadt. Combined differential and common-mode scattering parameters: theory and simulation. *IEEE Transactions on Microwave Theory and Techniques*, 43(7):1530–1539, July 1995. ISSN 0018-9480.

C. H. Chen, P. Davuluri, and D. H. Han. A novel measurement fixture for characterizing USB 3.0 radio frequency interference. In *Electromagnetic Compatibility (EMC), 2013 IEEE International Symposium on*, pages 768–772, Aug. 2013.

Kusum Deep and Manoj Thakur. A new mutation operator for real coded genetic algorithms. *Applied Mathematics and Computation*, 193(1):211–230, 2007.

W. Gao, L. Wan, S. Liu, L. Cao, D. Guidotti, J. Li, Z. Li, B. Li, Y. Zhou, F. Liu, Q. Wang, J. Song, H. Xiang, J. Zhou, X. Zhang, and F. Chen. Signal integrity design and validation for multi-GHz differential channels in SiP packaging system with eye diagram parameters. In *Electronic Packaging Technology High Density Packaging (ICEPT-HDP), 2010 11th International Conference on*, pages 607–611, Aug. 2010.

David E. Goldberg. *Genetic Algorithms in Search, Optimization and Machine Learning*. Addison-Wesley Longman Publishing Co., Inc., Boston, MA, USA, 1st edition, 1989. ISBN 0201157675.

R. F. Harrington. *Field Computation by Moment Methods*. The Macmillan Company, 1968.

J.H. Holland. Adaptation in natural and artificial systems. 1975.

Intel. USB 3.0* Radio Frequency Interference Impact on 2.4 GHz Wireless Devices, 2012. URL `http://www.intel.com/content/dam/www/public/us/en/documents/white-papers/usb3-frequency-interference-paper.pdf`. [2017-03-30].

Keysight. ADS - Advanced Design System, 2016. URL `http://www.keysight.com/find/eesof-ads`. [2017-03-30].

B. L. Miller and David E. Goldberg. Genetic algorithms, tournament selection, and the effect of noise. *Complex Systems*, (9):193–212, 1996.

Lars Nolle, R. Krause, and R. J. Cant. On practical automated engineering design. In K. Al-Begain and A. Bargiela, editors, *Seminal Contributions to Modelling and Simulation*. Springer, 2016.

David M. Pozar. *Microwave engineering*. J. Wiley & Sons, 4th edition, 2012. ISBN 978-0-470-63155-3.

N. Stevens and T. Dhaene. Generation of rational model based spice circuits for transient simulations. In *2008 12th IEEE Workshop on Signal Propagation on Interconnects*, pages 1–4, May 2008.

Gilbert Syswerda. Uniform crossover in genetic algorithms. In J. David Schaffer, editor, *ICGA*, pages 2–9. Morgan Kaufmann, 1989. ISBN 1-55860-066-3.

P. Triverio, S. Grivet-Talocia, M. S. Nakhla, F. G. Canavero, and R. Achar. Stability, causality, and passivity in electrical interconnect models. *IEEE Transactions on Advanced Packaging*, 30(4):795–808, Nov. 2007. ISSN 1521-3323.

J. Werner, J. Schütt, and G. Notermans. Sub-miniature common mode filter with integrated ESD protection. In *2015 IEEE International Symposium on Electromagnetic Compatibility (EMC)*, pages 386–390, Aug. 2015.

J. Werner, J. Schütt, and G. Notermans. Common mode filter for USB 3 interfaces. In *2016 IEEE International Symposium on Electromagnetic Compatibility (EMC)*, pages 100–104, July 2016.

Jens Werner and Lars Nolle. Spice Model Generation from EM Simulation Data Using Integer Coded Genetic Algorithms. In Max Bramer and Miltos Petridis, editors, *2016 SGAI*, pages 355–367. Springer International Publishing, Dec. 2016.